



# Solar PV Array Reconfiguration Scheme for Energy Extraction Enhancement in Grid-Connected PV Systems

S.Ravikumar<sup>1</sup>, E.Rajasekaran<sup>2</sup>

<sup>1</sup> Research Scholar & Assistant Professor, St.Michael College of Engineering and Technology, Kalayarkovil, Tamilnadu, India,

<sup>2</sup> Research Scholar & Assistant Professor, St.Michael College of Engineering and Technology, Kalayarkoil, India,

**Abstract**—This paper relates a dynamical electrical array reconfiguration (EAR) scheme on the photovoltaic (PV) generator of a grid-connected PV system based on a plant-oriented configuration, in order to develop its energy fabrication when the operating situations of the solar panels are different. The EAR scheme is carried out by injecting a controllable switching matrix between the PV generator and the central inverter, which allows the electrical recoupling of the offered PV modules. As a result, the PV system exhibits a self-capacity for real-time adaptation to the PV generator external operating situations and develops the energy extraction of the system. Experimental results are provided to validate the future approach.

**Index Terms**—Electrical array reconfiguration (EAR), gridconnected photovoltaic (PV) systems, reconfigurable PV systems.

Received 06 October, 2021; Revised: 18 October, 2021; Accepted 20 October, 2021 © The author(s) 2021. Published with open access at [www.questjournals.org](http://www.questjournals.org)

## I. INTRODUCTION

PHOTOVOLTAIC (PV) energy generation delivers several advantages such as being inoffensive for the environment and renewable. Furthermore, grid-connected PV energy generation represents a renewable energy-growing another that is becoming more competitive due to the new favorable governmental laws and policies recently introduced. For instance, most of the programs auxiliary PV systems have promoted, among others, the expansion of small residential PV systems up to 5 kWp connected to the single-phase grid primarily installed in roofs [1], [2].

The plant-oriented (PO) configuration is one of the most fundamental PV grid-connected system's plannings due to its simplicity and low cost per peak kilowatt, and assumes a single PV generator (or solar array) formed by a prefixed parallel connection of series-connected modules (also referred to as strings) which is linked to the grid through a single central inverter [1], [2]. The dc power extraction is carried out by the inverter input stage which is generally driven by a maximum power point tracking (MPPT) algorithm in charge to ensure the PV generator operation at its maximum power point whatever the environmental (irradiance and temperature) situations are.

One of the major sources of power losses in such planning arises when the PV generator is partially shaded by clouds or by nearby obstacles such as in the case of city environments [3]–[6]. These losses are mainly due to the electrical configuration of the PV generator, in particular to the hardwired series connection of PV modules in each string since a partially shaded module bounds the string current wherever it is connected, thus reducing the maximum offered dc power of the PV generator. Moreover, this power reduction can also occur in case of module failure for the same reasons.

In order to develop the dc power extraction of a partially shaded solar array, several solutions modifying either: 1) the power processing planning or 2) the PV generator electrical behavior at the solar cells level, have been future.

1) The scheme which modifies the power processing planning is based on a previous association of the offered PV modules in several self-governing PV generators. Each PV generator is formed by the PV modules operating under similar environmental situations to reduce the current limitation on the strings. Moreover, the dc power extraction is developed by a modified power processing planning which shares out the maximum dc power extraction task between as many power processors as self-governing PV generators are. Depending on

the number of PV generators, ac-module inverters [7], [8], string and multistring converters [9], [10], or cascaded full-bridge multilevel [11] topologies are some of the power processing plannings auxiliary this scheme. It is worth seeing that this approach develops the energy efficiency and the reliability of the PV system at expenses of increasing the power stage complexity and cost [12].

2) To avoid these drawbacks, other solutions modify the operation of the PV generator at the solar cells level when partial shades are present, keeping the power processing planning based on a single power processor (i.e., a single inverter in the case of the PO configuration). The most popular one is well known by the PV modules producers who provide the option to connect bypass diodes in parallel with some subsets of series-connected solar cells accumulated in the module. The PV module power develops since these diodes turn- on and release the series-connection current limitation when several of these cells are shaded. However, when bypass diodes are employed the power-to- voltage/current curves of the PV generator exhibit more than one maximum. Consequently, the maximum power extraction needs the use of more sophisticated MPPT algorithms able to disregard local maximums with respect to the absolute one. Unfortunately, commercial inverters rarely include these advanced algorithms [3].

An another approach based on an adaptive electrical array reconfiguration (EAR) of solar cells has been recently future in [13]. In this paper, the authors introduce a new configuration of the solar cells connections based on a hard-wired fixed part of total-cross-tied array and an adaptive one of self-governing solar cells, being both parts linked through a controllable matrix of switches. This matrix is controlled in real time to connect the less shaded cells of the adaptive part, in parallel with the more shaded rows of the fixed one. Hence, this reconfiguration scheme releases the array current limitation under partial shades and optimizes the output power. The proper operation of this scheme has been experimentally complete by the authors in the case of a reconfigurable array directly feeding a resistive load. However, this interesting approach needs the PV module producers commitment to be commercially offered in the future.

In contrast, the work here reported proposes a reconfiguration scheme at the PV module level which can be applied to commercial PO grid-connected PV systems offered nowadays, i.e., formed by standard PV modules and a single central inverter driven by a conventional MPPT algorithm. The future approach is partially inspired in the EAR applied to autonomous PV systems such as cars powered by solar energy

[14] and electric engines coupled to water pumps [15]–[17]. As earlier reported by the authors of this paper in [18]–[20] and following a similar way as done in [13], the reconfiguration scheme is based on a controllable matrix of switches configuring the PV modules in a single-string of parallel- connected rows connected to the central inverter. Under partial shades or in case of module failure, the matrix control algorithm reconfigures the PV modules to maximize the current of the single string, i.e., the output power of the system.

This paper extends the contents reported in [18]–[20] with a detailed description of the switching matrix design, its implementation, and control in Sections II and III, respectively. Section IV details the experimental setup of a commercial 1.65-kWp grid-connected PV system built following the future approach to test the proper operation of the scheme. Subsequently, Section V reports an extended set of experimental results to show the EAR PV system operation. Finally, the last section draws the conclusions of the paper and its contribution to the energy and reliability development of PV systems.

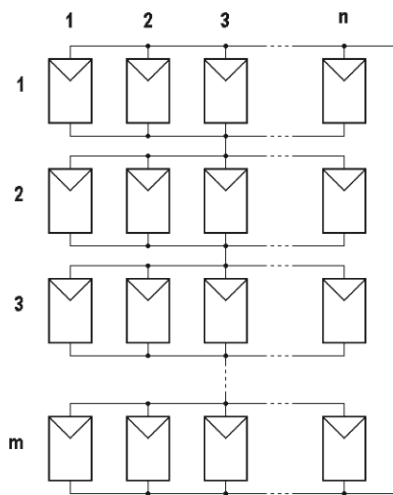


Fig. 1. EAR PV generator topology.

## II. SWITCHING MATRIX DESIGN

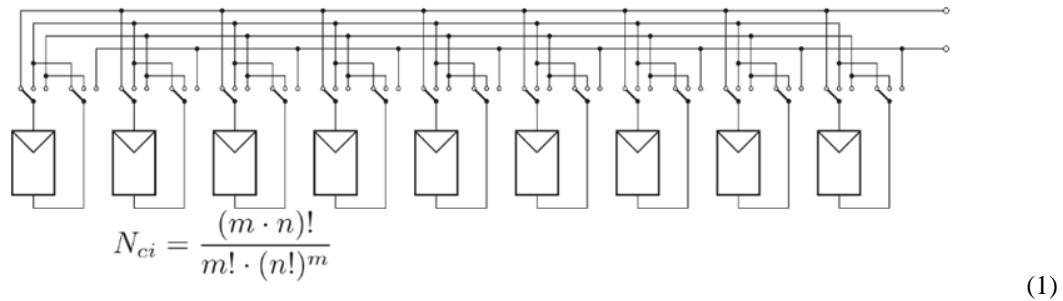
All the offered PV modules are accumulated in an  $m \times n$  matrix structure of a single string of  $m$  series-connected rows with  $n$  parallel-connected modules per row, as shown in Fig. 1, which will be referred as “EAR PV generator topology.”

It is worth noting that the maximum offered dc power at the output of the PV generator will depend on the operating situations of each module (i.e., irradiance, temperature, and electrical characteristics) and on their location in the matrix structure. This property can be used to maximize the dc output power by properly relocating the PV modules within the PV generator topology. This relocation can be carried out by injecting a switching matrix between the PV generator and the inverter, enabling at any time the parallel connection of any PV module in any of the  $m$  rows of the PV generator, thus preserving the structure of  $n$  modules per row. This design requirement can be achieved by using  $2 \cdot m \cdot n$  switches of single-pole  $m$ -throws, as shown in Fig. 2 for the case of  $m = 3$  rows and  $n = 3$  PV modules per row.

It can be pointed out that this structure can be expanded to increase the current and/or the voltage capabilities of the PV generator preserving the matrix structure: A current increase can be obtained by adding the same number of PV modules in each row, whereas a voltage increase will result from the addition of PV module rows to the single string.

On the other hand, the previous switching matrix enables  $(m \cdot n)!$  possible reconfigurations of the PV modules (i.e.,  $9! = 362880$  for the case of Fig. 2). However, as shown in Fig. 3, some of the possible configurations can be disregarded since both the module position in a row [Fig. 3(a)] and the row position in the single string [Fig. 3(b)] are irrelevant with respect to the delivered dc output power.

The configurations which can deliver different values of output power, assuming that the irradiances present on each module are different, will be referred as “configurations of interest.” For a PV generator with an  $m \times n$  matrix structure, the number of these configurations, noted as  $N_{ci}$ , is given by



$$N_{ci} = \frac{(m \cdot n)!}{m! \cdot (n!)^m} \tag{1}$$

Fig. 2. Switching matrix for  $m = n = 3$ . General case.

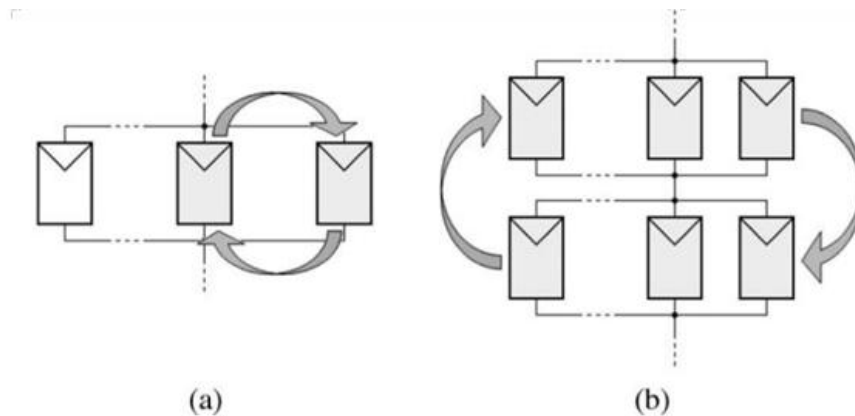


Fig. 3. Irrelevant configurations respect to the delivered dc power.

In particular, for the case wherever  $m = n = 3$  only 280 configurations of the 362880 ones can deliver different values of maximum dc power at the PV generator output. As a consequence, the number of switches needed to handle these 280 configurations can be reduced with respect to the general case, thus simplifying the switching matrix design. For instance, Fig. 4 shows the resulting simplified switching matrix for the previous case, wherever only 14 switches of 3 throws and 2 switches of 2 throws are needed instead of the 18 switches of 3 throws of Fig. 2.

### III. SWITCHING MATRIX CONTROL: RECONFIGURATION SCHEME

The reconfiguration scheme is based on the fact that, on one hand, the maximum power point (MPP) voltage has a small variation within a wide range of the irradiance on a PV module, and, on the other hand, that the MPP current of a PV module can be considered nearly proportional to the irradiance value.

Therefore, referred to the EAR PV generator topology, it can be concluded as follows.

- 1) The MPP voltage of parallel-connected PV modules will not be greatly affected by the value of the irradiance on each module.
- 2) The current flowing through a set of parallel-connected PV modules will be almost proportional to the amount of the irradiance values present on each module.

In order to maximize the offered power at the PV generator's output, it would be desirable that none of the seriesconnected rows of parallel-connected PV modules bounds the current flowing in the single string. This behavior can be achieved if the currents, and thus the irradiances, in the different rows are similar. This principle of operation is referred as "irradiance equalization" of the PV generator. Hence, the reconfiguration scheme is based on relocating the PV modules on the rows so that the irradiance equalization is achieved. This principle is shown in Fig. 5, wherever, starting from an initial configuration [Fig. 5(a)], the scheme relocates the modules 2 and 9 to equalize the average of the irradiances present at each row [Fig. 5(b)].

The flowchart of the algorithm implementing this reconfiguration scheme is shown in Fig. 6, and its main steps are described in the following.

#### A. Offline Computation: Setting Initial Situations

Starting from a PV generator formed by  $m \times n$  PV modules initially connected, as shown in Fig. 1, the algorithm assumes that the irradiance value of each module is known (or can be estimated, as is addressed later) and is noted as  $G_{ij}$ , wherever  $i = 1, \dots, m$  and  $j = 1, \dots, n$  stand for the row and the column, respectively, wherever the module is initially located. Once the values of  $m$  and  $n$  are known, and assuming that all the values of the irradiance  $G_{ij}$  are different, the algorithm computes offline all the configurations of interest defined in Section II. Each of these configurations is identified as  $A_k$ , wherever  $k = 1, 2, \dots, K$  (note that if  $m = n = 3$ , then  $K = 280$ ), and the corresponding irradiance of each module is noted as  $G_{ijk}$ .

#### B. Online Computation

1) *Irradiance Estimation:* The reconfiguration algorithm needs the knowledge of the irradiance on each module. Even though this parameter can be known by means of an irradiance sensor, it can anotherly be estimated from the measurements of the PV module voltage and current and the simplified solar panel electrical model given by

$$G_{ij} = \alpha \cdot \left[ I_{ij} + I_0 \cdot (e^{V_{ij}/nV_T} - 1) \right] \quad (2)$$

being  $G_{ij}$  the estimated irradiance,  $I_{ij}$  and  $V_{ij}$  the measured current and voltage, respectively, and  $\alpha$ ,  $I_0$ , and  $nV_T$  a set of parameters which can be evaluated from the values of the shortcircuit current, the open-circuit voltage, and the maximum power operating point of the PV module given in the data sheets of the manufacturer, respectively. As it is addressed in the next section, this option has been finally selected for the reconfigurable PV system design since from the measurements of the voltage and the current of each module a possible module failure can also be detected and taken into account by the reconfiguration algorithm to try to minimize the corresponding loss of dc power.

2) *Computation of Average Irradiance Present at Each Row:* For each of the configurations of interest  $A_k$ , the algorithm computes the average irradiance on the  $n$  parallel-connected

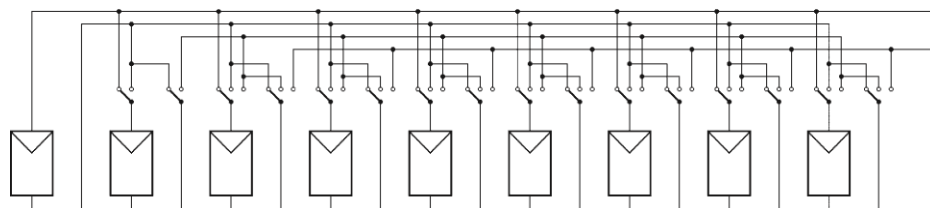


Fig. 4. Simplified switching matrix for  $m = n = 3$ .

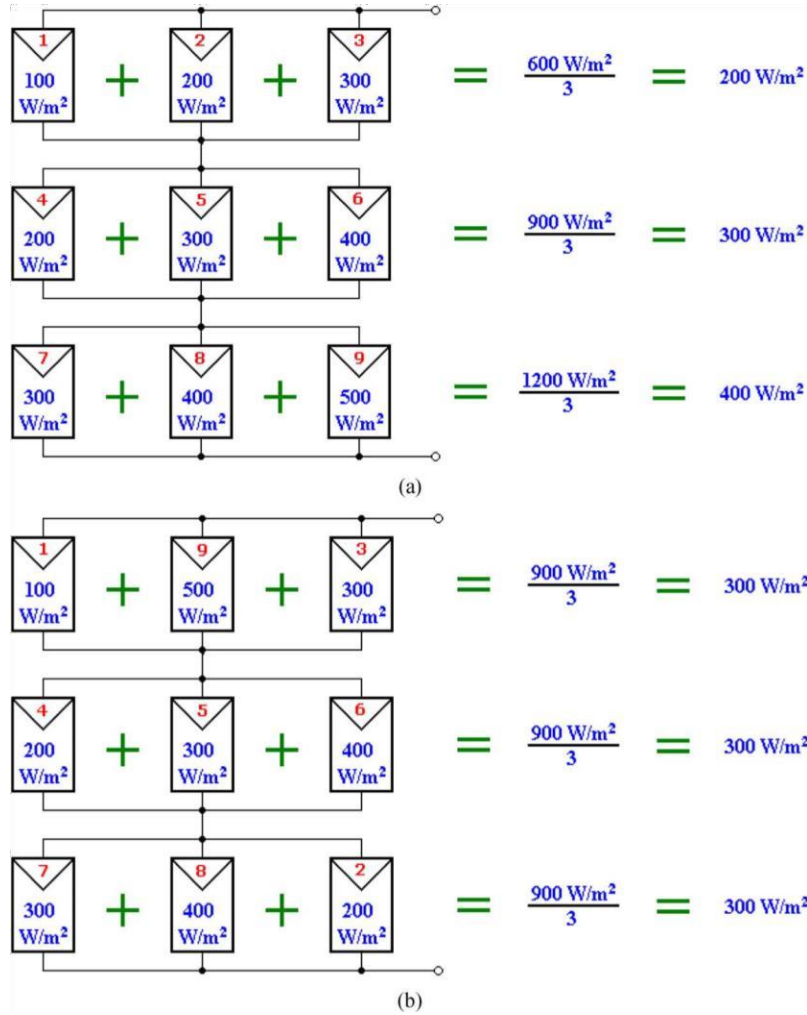


Fig. 5. Principle of the reconfiguration scheme. (a) Initial configuration. (b) Final configuration.

modules of each row. If  $G_{ik}$  stands for the average irradiance present at the row  $i$  of the configuration  $A_k$ , the algorithm computes

$$G_{ik} = \frac{\sum_{j=1}^n G_{ijk}}{n}, \quad i = 1, 2, \dots, m \quad k = 1, 2, \dots, K. \quad (3)$$

3) *Computation of "Irradiance Equalization Index":* In order to subsequently check which of the configurations of interest will deliver the maximum power, the algorithm computes for each configuration a merit factor called "irradiance equalization index." This index is defined to quantify how different are the average irradiances present at each row and consequently what is the degree of current limitation of the configuration. Even other definitions are possible, a simple way to define the irradiance equalization index of the configuration  $A_k$ , referred  $I_s$  consequently, the algorithm computes

$$M_{IE}(A_k) = \max[G_{1k}, G_{2k}, \dots, G_{mk}] - \min[G_{1k}, G_{2k}, \dots, G_{mk}] \quad \text{for} \quad k = 1, \dots, K. \quad (5)$$

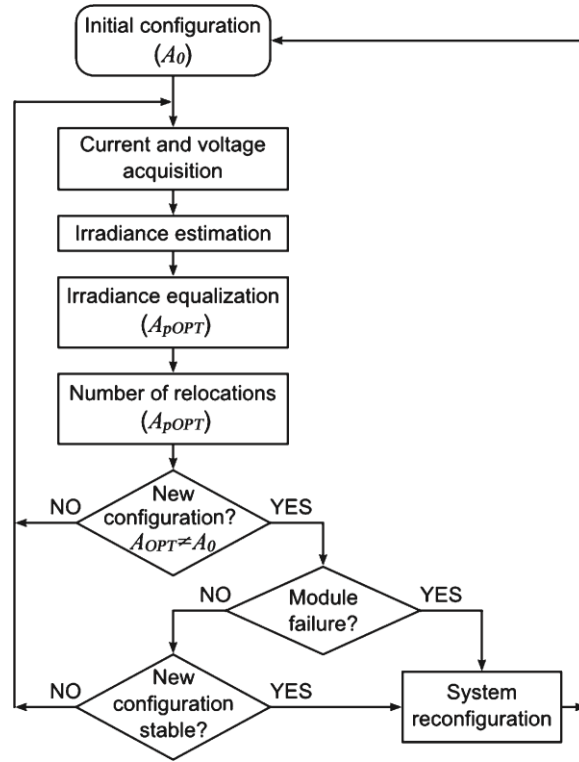


Fig. 6. Flowchart of the algorithm for the system reconfiguration.

It can be noted that the better the irradiance equalization, the lower the index value. In particular, if all the rows of a configuration exhibit the same average irradiance (i.e., irradiance equalized for each row), then,  $MIE(Ak) = 0$ , as in the case of a PV generator operating under an uniform irradiance.

As earlier mentioned, the computation of  $MIE(Ak)$  allows the algorithm to detect what configurations are optimal as regards the delivered maximum power. These configurations, noted as  $A_{pOPT}$  being  $p$  an integer, constitute a subset of the configurations of interest, namely,  $A_{pOPT} \in \{A1, A2, \dots, AK\}$  and can easily be detected by computing

$$MIE(A_{pOPT}) = \min[MIE(A1), MIE(A2), \dots, MIE(AK)]. \quad (6)$$

It can be pointed out that more than one configuration can result optimal.

4) *Computation of Number of PV Module Relocations:* In order to minimize the number of relocations, the algorithm computes for each optimal configuration a second merit factor defined as “number of relocations.”

This index evaluates the number of modules to be relocated when the PV generator is reconfigured from the current configuration  $A_0$  to the optimal one under analysis,  $A_{pOPT}$ . For instance, referring to Fig. 5, the “number of relocations” to carry out the reconfiguration from the initial configuration of Fig. 5(a) to the optimal one in Fig. 5(b) is two, and corresponds to the relocations of modules 2 and 9.

These previous steps will allow us to identify the optimal configuration noted as  $A_{OPT}$ , i.e., the configuration that concurrently better equalizes the irradiance and minimizes the

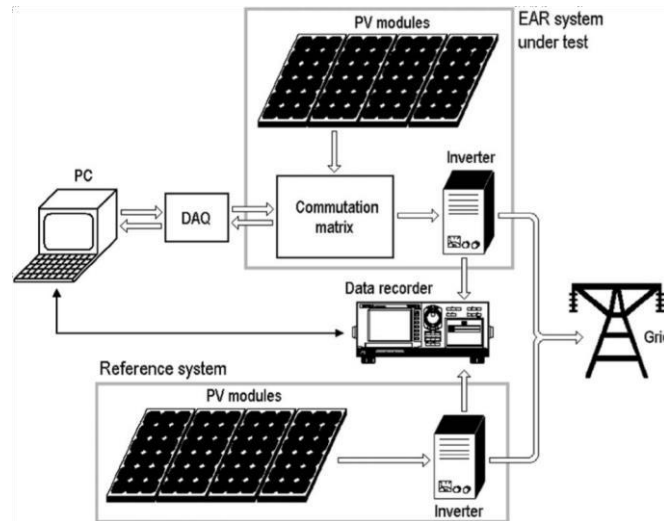


Fig. 7. Experimental setup.

number of module relocations. In the next step, the algorithm decides if the reconfiguration has to take place or not, as described in the following.

5) *Reconfiguration Decision Making*: As can be seen in the algorithm flowchart, the decision making is structured in three hierarchical levels, namely, as follows.

The first level of decision disables the reconfiguration of the switching matrix if the optimum configuration is the same that the initial one. Otherwise, the algorithm goes to the second decision level.

The second level asks for a possible module failure which can be detected from the measurement of the module current: If any module is in open circuit, the reconfiguration takes place immediately to avoid the possible disconnection of the PV generator at the inverter's input. Otherwise, the algorithm goes to the third decision level.

The third decision level enables the reconfiguration of the switching matrix only if the optimum configuration is stable (i.e., if it leftovers the same) during a certain amount of time. Once the optimum configuration is determined for the first time, the algorithm runs a prefixed number of turns and checks if this configuration leftovers unchanged to authorize the reconfiguration. Referring to the system implementation described later, the algorithm running time spends around 200 ms in one turn, including the data acquisition, the irradiance estimation, and the irradiance equalization procedure leading to the optimum configuration. In the third decision level, the algorithm has been programmed to run during 15 s, which means that the optimum configuration is recalculated 75 times before the reconfiguration takes place. As will be evidenced later by experimental results, this scheme avoids a large number of reconfigurations in front of fast irradiance changes on the PV generator, as in the case of cloudy days, and thereby preserves the lifetime of the switches.

In order to experimentally validate the assumptions above under a proof of concept basis, the next section describes a work bench formed by a 1.65-kWp PV grid-connected system including a switching matrix controlled by the irradiance equalization algorithm summarized earlier.



Fig. 8. Modules layout of the PV system. [R1...R6] Mention system. [S1...S4] Static section. [1...6] Reconfigurable section.

#### IV. EXPERIMENTAL SETUP

##### A. General Description

The setup shown in Fig. 7 has been built using commercial equipment, and includes a PV grid-connected mention system used to check the irradiance evolution during the tests, the EAR reconfigurable one, and processing and monitoring devices.

The setup components are described in the following.

- 1) Mention PV grid-connected system.
  - a) Five PV modules STP165S- 24/Aa (825 WP).
  - b) SB700 inverter from SMA (700 W).
- 2) Processing and monitoring facilities.
  - a) Personal computer which embeds the control algorithm and manages the recorded data.
  - b) Data acquisition system USB-6259 DAQ from National Instruments.
- 3) EAR PV system under test.
  - a) Relay-based switching matrix.
  - b) Ten PV modules STP165S-24/Aa (1650 WP). Each module includes 72 series-connected solar cells and two parallel-connected bypass diodes (one for each set of 36 cells).
  - c) SB1100 inverter from SMA (1100 W), including an MPPT algorithm that only runs within the inverter input voltage operating range, namely, from 139 to 400 V.

##### B. EAR PV Generator Design

In order to comply with the SB1100 inverter input voltage and current operating ranges, and to build a switching matrix of reduced size, the EAR PV generator includes a static section of four PV modules and a reconfigurable one of six modules formed by three series-connected rows of two parallelconnected modules per row, leading to a  $3 \times 2$  matrix structure. Fig. 8 shows the layout of the reconfigurable system with its static and reconfigurable parts as well as the mention system.

On the other hand, Fig. 9 shows the EAR PV generator configuration and the location of the auxiliary circuits to sense the current and the voltage of each module. In this regard, the voltage measurements are referred to a common node, to avoid

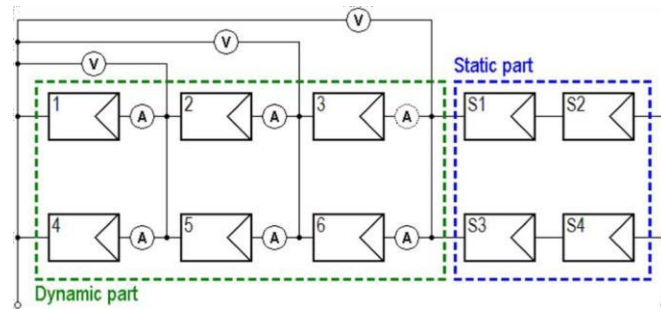


Fig. 9. EAR PV generator under test with the static section, the reconfigurable one, and the voltage and current sensors distribution.

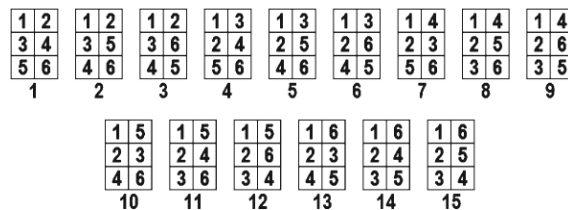


Fig. 10. Fifteen PV modules configurations of interest.

the use of differential amplifiers requiring high common mode rejection ratio values.

It can be noted that one current sensor can be omitted, since one current value comes from the application of Kirchoff laws.

##### C. Switching Matrix and Auxiliary Circuits Design

As addressed in the previous section, the switching matrix simplified design first needs the analysis of which configurations are of interest, i.e., which of them deliver different values of output dc power. For the case of study,  $m = 3$  and  $n = 2$ , thus only 15 configurations are of interest (i.e.,  $A_k$  with  $k = 1, 2, \dots, 15$ ) among the  $(3 \cdot 2)! = 720$  possible ones. Fig. 10 shows the location of the modules (numbered from one to six) in the



reconfigurable part of the EAR PV generator for each of these 15 configurations, wherever the PV modules in the same row are parallel connected and the three rows of PV modules are series connected.

The simplified switching matrix enabling the parallel connection of any PV module in any row is shown in Fig. 11 and includes two single-pole double-throw and four single-pole triple-throw switches.

Switching relays are good candidates to the implementation of these switches due to their control simplicity and the inherent electrical isolation operation of their control circuitry. From an efficiency point of view, bistable relays (or latching relays) are particularly well suited since they only spend energy to change their state. However, electromagnetic monostable relays have been finally included in the prototype since they control results simpler.

The electrical planning of the system is based on single dc bus connecting, on one hand, the static section and the inverter [see Fig. 12(a)]. On the other hand, the bus also feeds the switching matrix relays and the auxiliary circuits. Fig. 12(b) shows the dc bus, the six switches driving a single module connection as well

2) The second one matches the failure of several PV modules by disconnecting them from the PV generator.

3) The third one registers the daily operation of both systems, in order to evaluate the shadowing effect on the PV generator due to the nearby buildings.

The identification of the EAR PV modules and the configurations of interest addressed in these tests correspond to the numeration given in Fig. 9. The initial connection of the modules corresponds to the configuration 1 of Fig. 10. The obtained results are described next:

#### A. PV Generator Operating Under Partial Shades

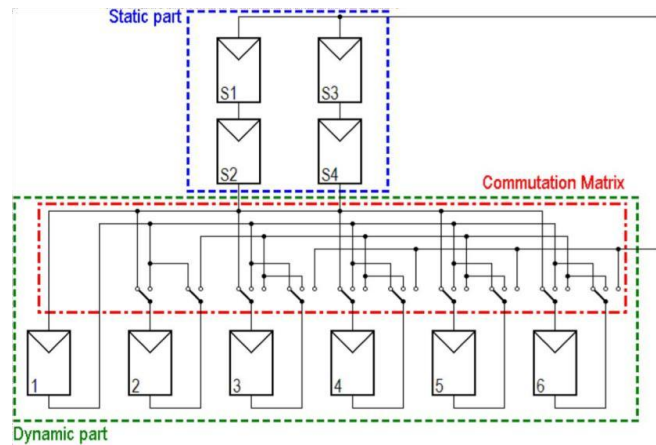


Fig. 11. EAR PV generator under test with the static section, the dynamically reconfigurable one, and the simplified commutation matrix.

as its corresponding current sensing circuitry implemented by means of a Hall-effect current transducer. Fig. 12(c) shows the voltage measurement circuitry across the module terminals (see also Fig. 8).

The PV modules current and voltage measured values are sent through the USB-6259 DAQ to the PC which subsequently computes using MATLAB software the reconfiguration algorithm driving the switching matrix.

As earlier reported in Section III, the algorithm running time spends around 200 ms in one turn.

Finally, the dc output power of the mention system and the EAR one is measured and registered for offline analysis by means of the WT1600 power meter. In this regard, since both grid-connected inverters include their own MPPT algorithm, it is assumed that the measured static output dc power corresponds to the maximum one.

## V. EXPERIMENTAL RESULTS

Three tests have been performed to check the proper operation of the equalization irradiance algorithm and the subsequent reconfiguration of the solar array.

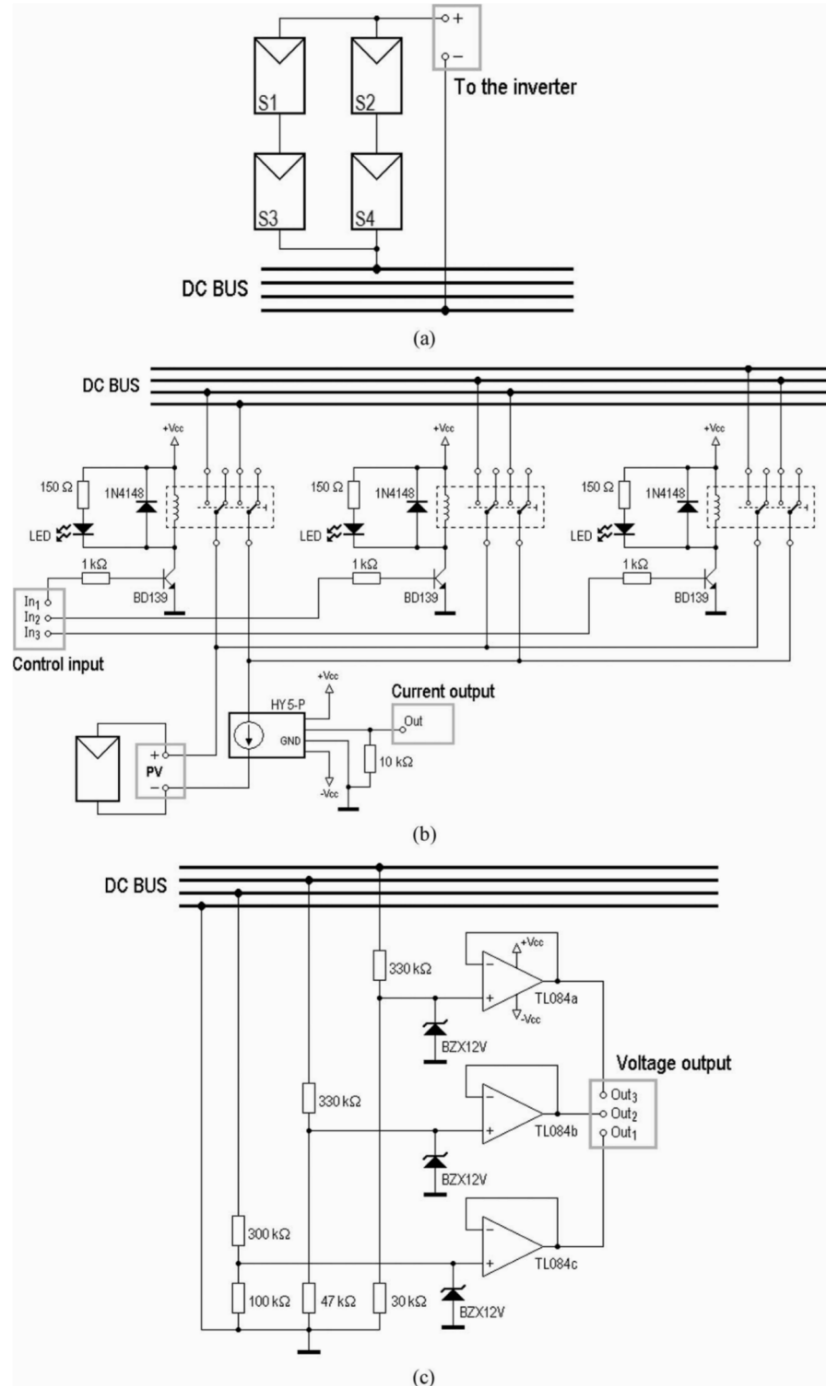
1) The first one artificially shades several PV generator modules.

This test hollowly shades one, two, or three modules of the EAR PV generator and drives the matrix to sequentially implement the 15 configurations of interest.

The power to voltage curve of each PV generator configuration is obtained to evidence the existence of optimal configurations that exhibit a maximum within the MPPT voltage window wherever the inverter operates (the lower limit of this window is shown in the curves and is noted as  $V_{MPP-min}$ ).

Fig. 13(a) corresponds to the case wherever a single module is shaded (module 1 in Fig. 9); as it can be seen, none of the 15 configurations results optimal since all the configurations lead to the same  $P-V$  curve. In contrast, Fig. 13(b) and (c) corresponds to the tests when the modules 1 and 4, and the modules 1, 4, and 6 are, respectively, shaded, and show that, in both cases, several configurations exhibit a maximum within the MPPT voltage window, and thereby result optimal. Referring to Fig. 10, these optimal configurations correspond to the case when the shaded modules are not parallel connected in the same row.

**B. Modules Failure in PV Generator**



For this test, the modules disconnection sequence shown in Table I is applied. This sequence emulates the failure of several modules of the PV generator.

Fig. 14 shows the measured dc output power of both the mention PV system and the EAR PV system under test when the switching matrix control is as follows: 1) activated and 2) disabled. These measurements evidence the power development of the EAR PV generator.

C. PV Generator Daily Operation

Two tests have been carried out to evaluate the EAR system daily operation: The first one, earlier reported in [20], focuses on the energy balance development of the system and the second one checks the number of reconfigurations under different weather situations to evaluate the operation of the reconfiguration algorithm as regards the switches lifetime. These tests are described next.

1) *Energy Development:* This test is devoted to quantify the daily energy development of the EAR-based system, when

Fig. 12. Electrical planning of the EAR PV generator.

the PV generator is affected by the shadows coming from the nearby buildings. Nevertheless, the offered PV panels at the laboratory are not enough to build both a static PV system and an EAR-based reconfigurable one which are required for a simultaneous comparison. Anotherly, this comparison has been done over the single EAR-based system during two consecutive sunny days of similar irradiance levels, enabling the switching matrix control during the first day, and disabling it during the second one in order to emulate a nonreconfigurable (i.e., static) PO PV system.

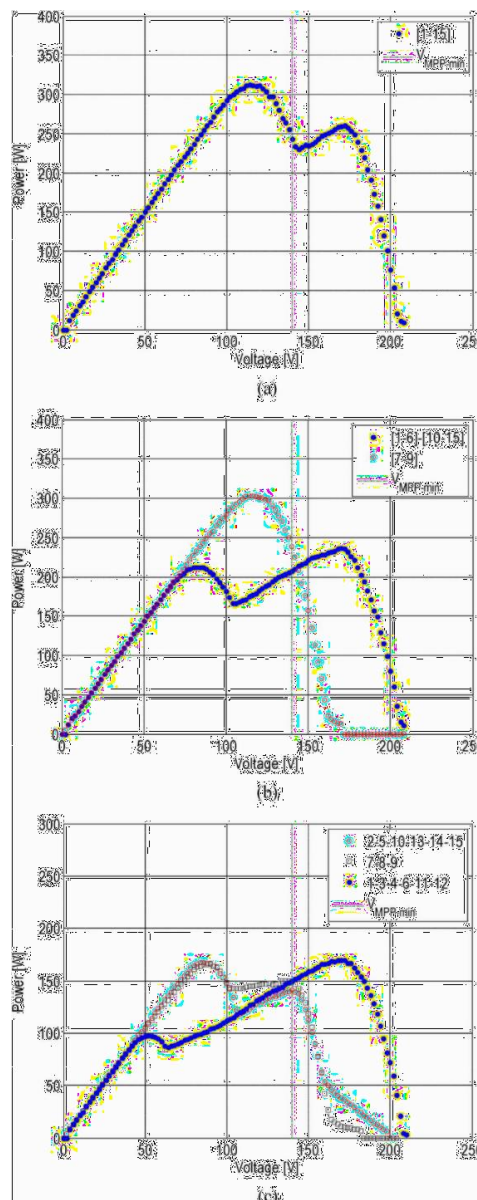


Fig. 13. Output power for EAR PV system under situations of shadow. (a) Shadow on module number 1. (b) Shadow on modules number 1 and 4. (c) Shadow on modules number 1, 4, and 6.

Fig. 15(a) shows the output power evolution during the day 02-22-2008 wherever the switching matrix control is enabled and reconfigures the PV generator according to the equalization irradiance algorithm. Similarly, Fig. 15(b) shows the output power of the day 02-23-2008 wherever the switching matrix control disabled. It is worth noting that the energy consumption of the EAR system must be subtracted from the measured value of  $\bar{E}_{EARON}$  since in the present design this system is not supplied by the PV modules. However, a measurement of the laboratory

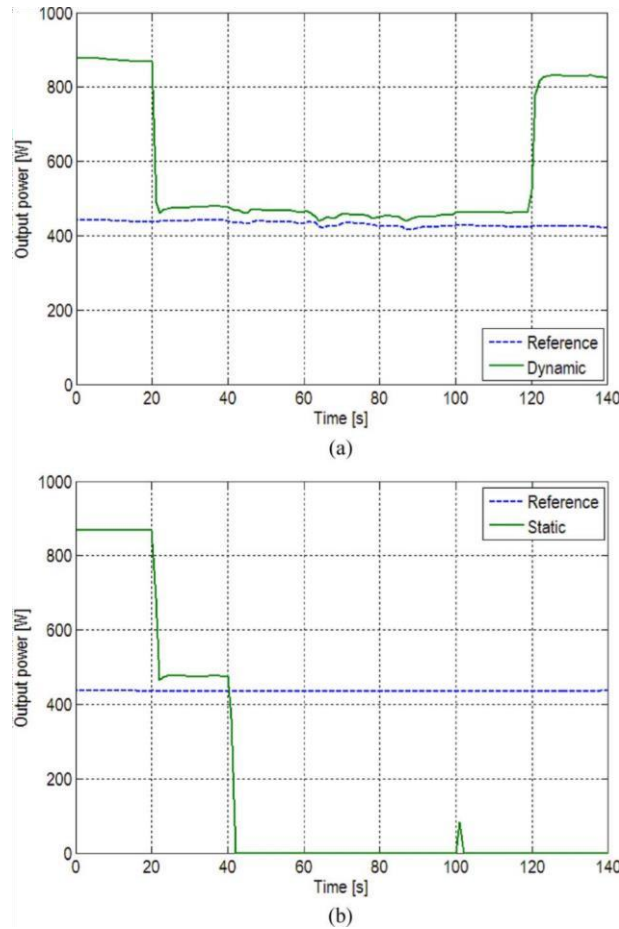


Fig. 14. EAR PV system output power when the switching matrix control is as follows:

(a) activated and (b) disabled.

prototype consumption may not be representative since the reconfiguration algorithm has been implemented on a PC, and monostable relays have been used instead of bistable ones. Anotherly, assuming the same implementation as presented earlier but based on bistable relays and wherever the PC is replaced by a low-cost microcontroller, the EAR system power consumption can be estimated from the data sheets of producers. In this regard, two kinds of power consumptions can be estimated, namely, as follows.

1) Standby power consumption: This refers to the consumption of the data acquisition system, the sensors/

TABLE I

SEQUENCE FOR PV MODULES FAILURE EMULATION conditioning circuits, and that corresponding to a lowcost microcontroller, for instance, the ATmega16 from ATMEL. The overall consumption of this equipment can be estimated around 1.2 W. Hence, if the PV system operates during 16 h a day in average, the standby energy consumption value can be estimated around 20 W · h a day. This consumption is the minimum one required by the EAR system to operate even if no reconfiguration takes place.

2) Bistable relay switching consumption: A change of the relay state needs about 20 W during 20 ms [21], [22], which means a power consumption of 0.12 mW · h per switching. This value can be neglected since at least 2000 switches a day would be required to spend less than 1% of the standby power consumption.

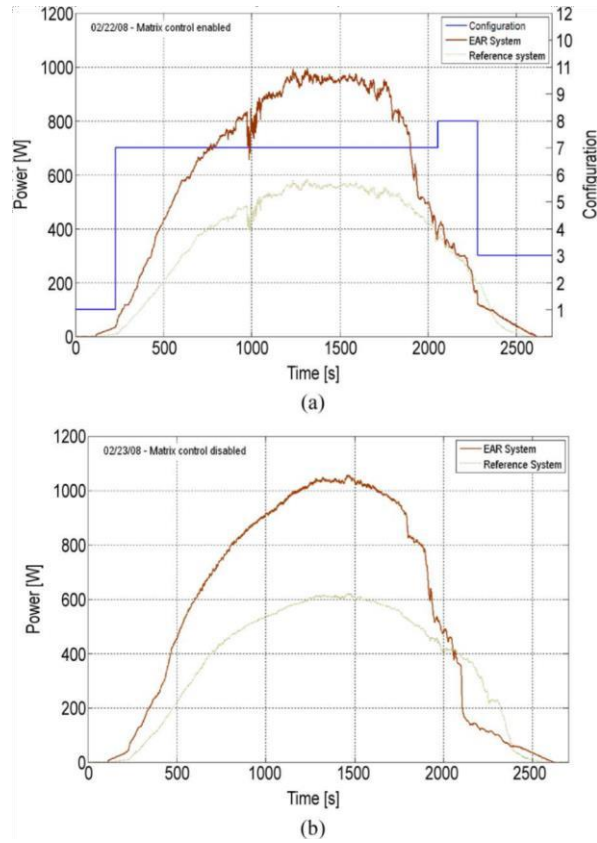


Fig. 15. Output power of EAR system and mention system when the control of the EAR system is as follows: (a) enabled and (b) disabled.

TABLE II  
ENERGY DELIVERED TO MAINS FOR PV SYSTEMS

| System    | Energy delivered to the mains       |                                      |
|-----------|-------------------------------------|--------------------------------------|
|           | Day 1 (02-22-08)<br>Control enabled | Day 2 (02-23-08)<br>Control disabled |
| EAR       | $E_{EAR_{ON}} = 5752.7 \text{ Wh}$  | $E_{EAR_{OFF}} = 6025.4 \text{ Wh}$  |
| Reference | $E_{REF_1} = 3539.0 \text{ Wh}$     | $E_{REF_1} = 3818.7 \text{ Wh}$      |

The energy injected to the mains during each of these two days taking into account these power consumption estimations, is reported in Table II, wherever  $E_{EAR_{ON}}$  and  $E_{EAR_{OFF}}$  stand for the

| Time (s) | Action                                    |
|----------|---|
| 0        | System connection with configuration n° 1 |
| 20       | Module 1 disconnection                    |
| 40       | Module 2 disconnection                    |
| 60       | Module 6 disconnection                    |
| 80       | Module 6 reconnection                     |
| 100      | Module 2 reconnection                     |
| 120      | Module 1 reconnection                     |
| 140      | End of test                               |

delivered energy when the switching matrix control is enabled or disabled, respectively.

From the results of Table II, it must be pointed out that the absolute values of the delivered energy by the EAR system when the switching matrix is either enabled or disabled cannot be directly compared since the irradiance level evolution is not strictly the same during the two days, as it can be checked from the energy values of the mention system. In this regard, the comparison can be made by using the normalized energy values of the EAR system with respect to the corresponding mention ones, namely

$$\frac{E_{\text{EAR}_{\text{ON}}}}{E_{\text{REF}_1}} = 1.626 \quad \frac{E_{\text{EAR}_{\text{OFF}}}}{E} = 1.578 \quad (7)$$

REF2

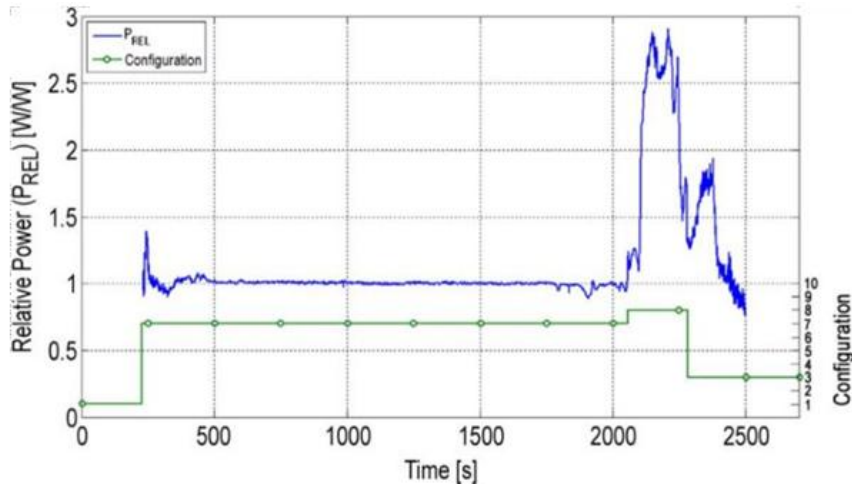


Fig. 16. EAR PV system relative output power.

which means that the EAR-based reconfigurable system delivers  $1 - (1.578/1.626) \approx 3\%$  more energy than the static one.

Anotherly, the comparison can also be performed in terms of the output power evolution, by comparing the output power of the static PV generator with that of the reconfigurable one, scaled by the power ratio of the mention system during the two days, namely: If  $PEAR_{\text{ON}}(t)$  and  $PEAR_{\text{OFF}}(t)$  stand for the EAR system power evolution when the switching matrix control is enabled or disabled, respectively, and  $P_{\text{REF}_1}(t)$ ,  $P_{\text{REF}_2}(t)$  correspond to the power evolution of the mention system during the two days, the relative power  $P_{\text{REL}}(t)$  can be defined as

$$P_{\text{REL}}(t) = \left. \begin{aligned} & \frac{PEAR_{\text{ON}}(t)}{P_{\text{REF}_1}(t)} \\ & \frac{PEAR_{\text{OFF}}(t)}{P_{\text{REF}_2}(t)} \end{aligned} \right\}$$

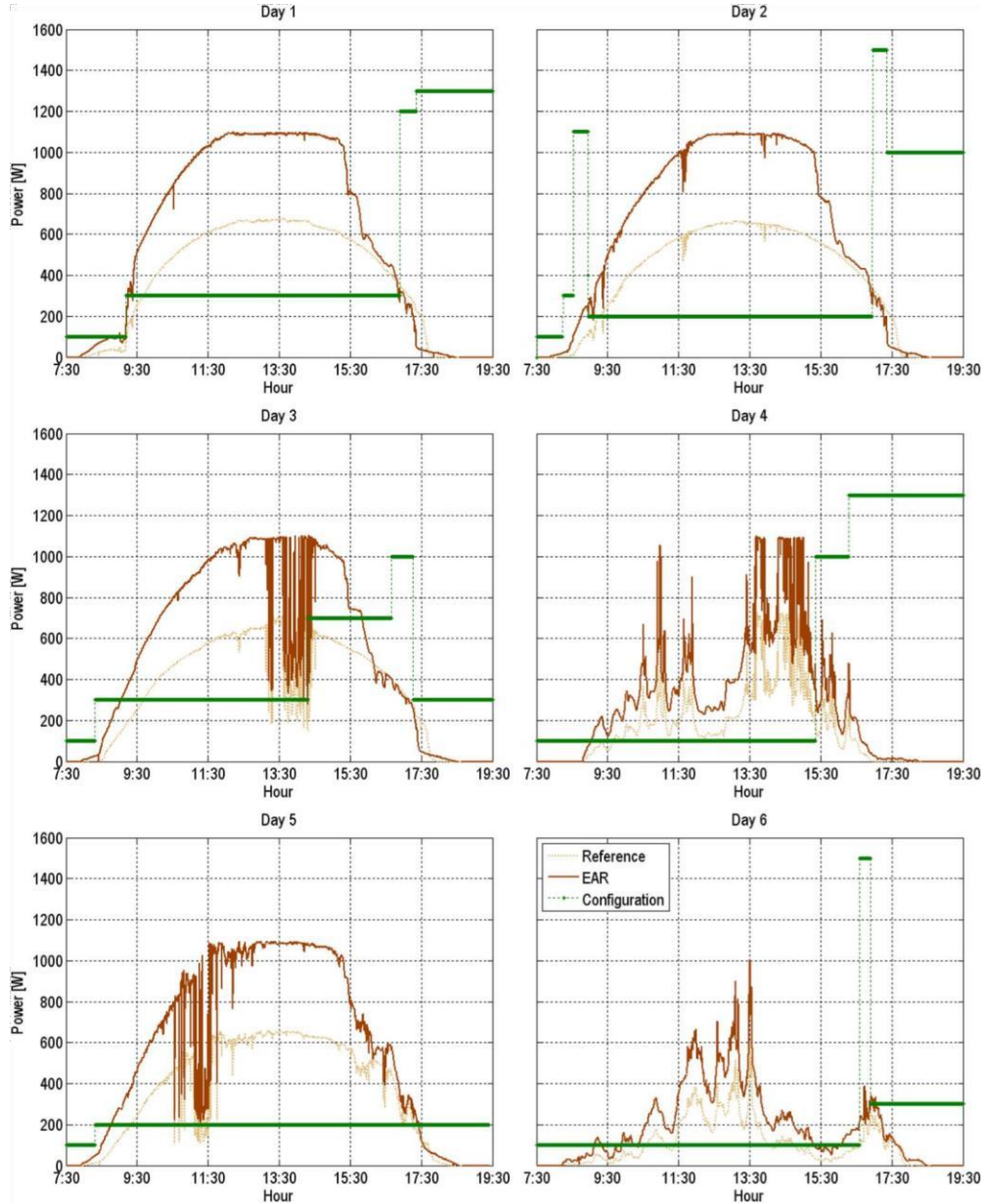


Fig. 17. Output power of EAR and mention system.

$$P_{PREL}^{OFF}(t) = \frac{P}{P_{REF2}(t)} \Rightarrow P_{REL}(t) = \text{OFF} \quad (8)$$

Fig. 16 shows the output power evolution of  $P_{REL}(t)$ , wherever the results at the beginning and end of the day are not representative due to overflow phenomena in the computation procedure.

It is worth noting that the plots of power evolution give us more information about the reconfiguration process: As it can be seen from Figs. 15 and 16, the power increase of the EAR system starts around  $t = 2050$  s, when the EAR PV generator is reconfigured from combination 7 to 8, and around  $t = 2300$  s, when the system is reconfigured from combination 8 to 3. The proper operation of the reconfiguration algorithm is complete by Fig. 8 which shows the first shades distribution over the EAR generator coming from the nearby buildings at  $t = 2050$  s when the first relevant reconfiguration takes place.

As it can be seen, panels 5 and 6 are fully and partially shaded, respectively; since, referring to Fig. 9, the initial combination of the EAR PV generator is the number 7, both panels are parallel connected, thus limiting the overall current of the PV generator.

The reconfiguration algorithm then elects the combination number 8 wherever both panels are now series connected, in order to develop the PV generator output power by relaxing the previous current limitation.

2) Number of Reconfigurations Under Different Weather Situations: The EAR system has been monitoring during one week wherever the weather was variable, including both sunny and cloudy days. Fig. 17 shows the power evolution of both the mention system and the EAR one. As it can be seen, at most five reconfigurations have been taken place during the day 02. It can be concluded that the number of reconfigurations in this test leftovers low.

## VI. CONCLUSION

This paper has submitted a PV generator reconfiguration scheme to develop the power of viable PO gridconnected PV systems offered nowadays, formed by standard PV modules and a single central inverter driven by a conventional MPPT algorithm. This scheme is executed by means of a controllable matrix of switches configuring the PV modules in a single-string of parallel-connected rows connected to the essential inverter. A set of experimental results carried out under a proof of concept basis on a small-scale grid-connected PV system of 1.65 kWp has shown both the viability of the approach and the resulting development of the provided power under partial shades or in case of module failures.

In spite of the disadvantages derivative from its greater complexity and cost, the power loss mitigation of this approach can result stimulating for small-scale installations in city environments wherever the PV generator can work under locations of severe partial shadows projected by nearby obstacles.

Finally, it can be pointed out that given a switching matrix the installed PV power can be expanded since the same matrix can also handle associations of hard-wired series-parallel modules instead of single ones, this being a subject of advance research.

## MENTIONS

- [1]. C. S. Chiu, "T-S fuzzy maximum power point tracking control of solar power generation systems", IEEE Transactions on Energy Conversion, pp. 1123-1132, 2010.
- [2]. L. A. Mozelli, R. M. Palhares, F. O. Souza, and E. M. Mendes, "Reducing conservativeness in recent stability conditions of TS fuzzy systems", Automatica 45 (2009), pp. 1580-1583, 2009.
- [3]. D. Saifia, M. Chadli, and S. Labiod, "Robust  $H_\infty$  static output feedback stabilization of T-S fuzzy systems subject to actuator saturation", International Journal of Control, Automation and Systems, vol. 10, no. 3, pp. 613-622, 2012.
- [4]. M. Drif, P. J. Pérez, J. Aguilera, and J. D. Aguilar, "A new estimation method of irradiance on a partially shaded PV generator in grid-connected photovoltaic systems," *Renew. Energy*, vol. 33, no. 9, pp. 2048-2056, Sep. 2008.
- [5]. C. Rodriguez and G. A. J. Amaratunga, "Long-lifetime power inverter for photovoltaic AC modules," *IEEE Trans. Ind. Electron.*, vol. 55, no. 7, pp. 2593-2601, Jul. 2008.
- [6]. B. Sahan, A. N. Vergara, N. Henze, A. Engler, and P. Zacharias, "A singlestage PV module integrated converter based on a low-power currentsource inverter," *IEEE Trans. Ind. Electron.*, vol. 55, no. 7, pp. 2602-2609, Jul. 2008.
- [7]. E. Roman, R. Alonso, P. Ibanez, S. Elorduizapatarietxe, and D. Goitia, "Intelligent PV module for grid-connected PV systems," *IEEE Trans. Ind. Electron.*, vol. 53, no. 4, pp. 1066-1073, Aug. 2006.
- [8]. N. Femia, G. Lisi, G. Petrone, G. Spagnuolo, and M. Vitelli, "Distributed maximum power point tracking of photovoltaic arrays: Novel approach and system analysis," *IEEE Trans. Ind. Electron.*, vol. 55, no. 7, pp. 2610-2621, Jul. 2008.
- [9]. J. A. Barrena, L. Marroyo, M. A. R. Vidal, and J. R. T. Apraiz, "Individual voltage balancing scheme for PWM cascaded H-bridge converterbased STATCOM," *IEEE Trans. Ind. Electron.*, vol. 55, no. 1, pp. 21-29, Jan. 2008.
- [10]. M. Calais, J. Myrzik, T. Spooner, and V. G. Agelidis, "Inverters for singlephase grid connected PV systems—An overview," in *Proc. IEEE 33rd Annu. PESC*, Cairns, Australia, Jun. 2002, vol. 4, pp. 1995-2000.
- [11]. D. Nguyen and B. Lehman, "An adaptive solar photovoltaic array using model-based reconfiguration algorithm," *IEEE Trans. Ind. Electron.*, vol. 55, no. 7, pp. 2644-2654, Jul. 2008.
- [12]. Y. Auttawaitkul, B. Pungsiri, K. Chammongthai, and M. Okuda, "A method of appropriate electric array reconfiguration management for photovoltaic powered car," in *Proc. IEEE APCCAS*, Chiangmai, Thailand, Nov. 1998, pp. 201-204.
- [13]. Z. M. Salameh and C. Liang, "Optimum switching point for array reconfiguration controllers," in *Proc. IEEE 21st PVSEC*, Kissimmee, FL, May 1990, vol. 2, pp. 971-976.
- [14]. Oscar Lopez-Lapena, Maria Teresa Penella and Manel Gasulla, "A New MPPT Method for Low-Power Solar Energy Harvesting", IEEE 2010
- [15]. Ahmed G. Abo-Khalil, "MPPT Control of Wind Generation Systems Based on Estimated Wind Speed Using SVR" IEEE 2008.
- [16]. Da-EunJeong "MYousefmuhammed," "An Enhanced MPPT Method Combining Model-Based and Heuristic Techniques" IEEE 2016PPT control of photovoltaic system using optimization voltage with temperature", IEEE 2012
- [17]. Silipa Sreekumar, "Maximum power point tracking of photovoltaic system using Fuzzy Logic Controller based boost converter", IEEE 2014